Available online at www.sciencedirect.com

ScienceDirect

journal homepage: http://www.elsevier.com/locate/acme

Original Research Article

On the influence of repetitive corrugation and straightening on the microstructure and mechanical properties of AA 8090 Al-Li alloy

Jenix Rino J *, *Balasivanandha Prabu S*, *Padmanabhan K. A*

Department of Mechanical Engineering, College of Engineering Guindy, Anna University, Chennai 600025, India

ARTICLE INFO

Article history:
Received 27 March 2017
Accepted 16 July 2017
Available online 9 August 2017

Keywords:
Severe plastic deformation
Grain refinement
Repetitive corrugation and straightening
Corrugation profiles
Mechanical properties

ABSTRACT

This paper reports on the improvements in the mechanical properties of AA8090 Al-Li alloy subjected to repetitive corrugation and straightening (RCS). AA 8090 Al-Li alloy sheets were processed using different corrugation profiles (semi-circular, flat-groove and V-groove) at 300 °C, with a pressing velocity of 2.5 mm/s. This study shows that a V-grooved die favors grain refinement, e.g. a reduction in the average grain size from 65 μm to 12 μm after eight passes is achieved. Grain size distribution and misorientation between grain boundaries were studied using EBSD and TEM. The microstructures also appear to have more high-angle grain boundaries in the case of the specimen processed using the V-grooved die. The tensile strength increases with the number of passes, but drops when surface cracks appear after the 16th pass for a semi-circular die, the 12th pass for a flat grooved die and the 10th pass for a V-grooved die. In contrast, the hardness continues to increase with increasing number of passes. Ultra-fine-/nano-grains were present after the eighth pass in a sheet that was processed using a V-grooved die.

© 2017 Politechnika Wrocławska. Published by Elsevier Sp. z o.o. All rights reserved.

1. Introduction

Enhancement of mechanical properties of metallic materials for multi-functional applications is an area of serious research [1]. Processes such as solid-solution strengthening, precipitation strengthening and strain hardening are employed to improve material properties by thermal/mechanical treatments. Severe plastic deformation (SPD) is a well recognized technique of relatively recent origin for producing ultrafine-/nano-grain structures in metallic materials. The generation of a high density of dislocations during severe plastic deformation leads to the formation of short to long range plastic strain bands, which eventually get converted into new grains. However, following SPD there is no significant overall dimensional change in the specimen [2]. In recent years, techniques such as equal channel angular pressing (ECAP) [3], high pressure torsion (HPT) [4], accumulated roll bonding (ARB) [5], multi-axial forging (MAF) [6], twist extrusion (TE) [7], repetitive upsetting extrusion (RUE) [8], rotary-die

* *Corresponding author.*
E-mail addresses: jenixproject@gmail.com (J.R. J), sivanandha@annauniv.edu (B.P. S).
http://dx.doi.org/10.1016/j.acme.2017.07.006
1644-9665/© 2017 Politechnika Wrocławska. Published by Elsevier Sp. z o.o. All rights reserved.

ECAP [9], cyclic extrusion and compression (CEC) [10], cyclic closed-die forging (CCF) [11], repetitive corrugation and straightening (RCS) [12] and some other integrated processes [13] are being used to improve the mechanical properties by the principal mechanism of grain refinement. Of these, ARB and RCS are suitable methods for producing ultrafine grain-/nano-structures in sheet materials. But, ARB has a limitation that during processing a good bonding between the stacked sheets does not always develop [14].

Al-Li alloys are used in several aerospace structural applications with a view to reducing the weight without compromising on engineering requirements, e.g. for use in the skin of aircraft wings [15]. The addition of 1 wt.% of lithium in aluminum reduces the weight of the component by 3% and increases the specific strength by 6% [16]. However, the strength of these alloys at high temperatures reduces as the metastable δ' phase Al_3Li and Al_2Li_3 dissolve at higher temperatures and facilitate recovery and grain growth [17], i.e. the stability of the material at high temperatures is a matter for concern.

Llorca-Isern et al. [18] have reported a significant improvement in the hardness of AA8092 Al-Li alloy at the end of four ECAP passes, i.e. from 660 MPa to 1378 MPa. Gao et al. [19] have reported that pre-stretching and aging of 2A97 Al-Li alloy plates increases their UTS from 447.7 MPa to 534.3 MPa. Despite the improvement in the ECAP process being high, this process cannot be scaled up beyond intermediate levels of production. In addition, specimens can be produced only in batches and there is also a limitation on the maximum possible dimensions. Therefore, an alternate, continuous process, namely, repetitive corrugation and straightening was studied here. This process is continuous and allows a scale up for large scale industrial production, if other factors are also made favorable by suitable improvements from the present levels. While it is expected that material properties would be improved significantly in this process also, as in the other SPD processes, research reports on this process are rather limited, especially those involving Al-Li alloys. Therefore, figures on the different relevant features are missing. In view of the above, this study reports on the effects on microstructure and mechanical properties of AA8090 Al-Li alloy of the repetitive corrugation and straightening process carried out with dies of different corrugation geometries at 300 °C. A somewhat similar study was presented earlier [20]. The differences between the two investigations of different focus were as follows: The material studied earlier was the Al-Mg (AA5083) alloy and the present study considers the Al-Li (AA8090) alloy, and the microstructure-correlations in these alloys are not identical. Therefore, the issues considered are similarity of observations between the two alloys and the differences. The overall aim is to broad base the conclusions. It was seen that AA5083 is ductile and isotropic whereas AA8090 is stiffer and anisotropic. Moreover, the present study considers the failure strain as a function of the experimental conditions and the homogeneity of grain refinement by measuring the hardness distribution. Furthermore, for the understanding of grain refinement mechanism, this study discusses the step by step metallurgical changes due to every successive two passes for the samples processed through the optimal die (V-groove) using TEM analysis.

2. Material and processing

AA8090 sheets of composition Al-94.46%, Li-2.5%, Si-1.8%, Cu-.5%, Zn-.171%, Ni-0.165%, Pb-0.387% (determined by spark atomic emission spectroscopy ASTM E1251-11) were supplied by ALCOA, Germany. Samples of dimensions 61 mm × 21 mm × 2 mm were prepared for the RCS process. These specimens were processed on a 50 T hydraulic press using three different dies, viz. a semi-circular die (radius 10 mm), a flat groove die (flank distance 5 mm, flank height 3 mm and corrugating angle 30°) and a V-groove die (pitch 20 mm, corrugating angle 30° and curve radius 2 mm). The different dies used for the experiments are shown in Fig. 1. The hydraulic press used in this RCS process is facilitated with a heating chamber mounted over the bed of the press, where a thermocouple is connected with a PID controller which has an indicator to ensure the working temperature (Fig. 2). The influence of temperature was also considered in this study. The material could not be processed at room temperature (RT), 100 °C and 200 °C because in these cases surface cracks were observed even after the first pass. High temperature DSC was used to determine the recrystallization temperature of the material – Fig. 3. The results indicate that the recrystallization temperature is ~350 °C. Therefore, the RCS processing temperature was kept at 300 °C, clearly below the recrystallization temperature. The ram velocity was fixed as 2.5 mm/s. The imparted strain on the specimen was measured along the longitudinal direction. The strain values are presented in Table 1. A corrugation – straightening step is considered as one pass. On each corrugated die the specimens were processed up to the maximum possible number of passes before failure. The specimens were processed to a maximum of 16 passes using the semi-circular die, 12 passes using the flat groove die and 10 passes using the V-groove die.

The theoretical values of the strain (ε) imparted were calculated using the formulae given below.

For a semi-circular corrugated die [21], the strain imparted in each pass can be calculated using Eq. (1).

$$\varepsilon = n\frac{4}{\sqrt{3}}\left(\frac{r+t}{r+.5t}\right) \tag{1}$$

For a flat groove die (shear in lateral and transverse directions are assumed to be negligible) [22], the strain imparted in each pass is calculated using Eq. (2).

$$\varepsilon = \frac{\Delta x/d}{\sqrt{3}} \tag{2}$$

where n = number of passes, r = radius of semi-circular die, t = thickness of the specimen, Δx = flank width and d = flank height.

The theoretical strain imparted using a V-groove die was calculated trigonometrically, assuming uniform deformation. The actual strain imparted in each case was measured experimentally by the optical grid analysis method [20]. The difference between the actual and the calculated strain is due to the theoretical calculations not considering the material behavior, kinematic hardening, temperature effect and frictional forces at the interfaces of the metal sheet and the die profile. In contrast, the experimental values reveal the actual

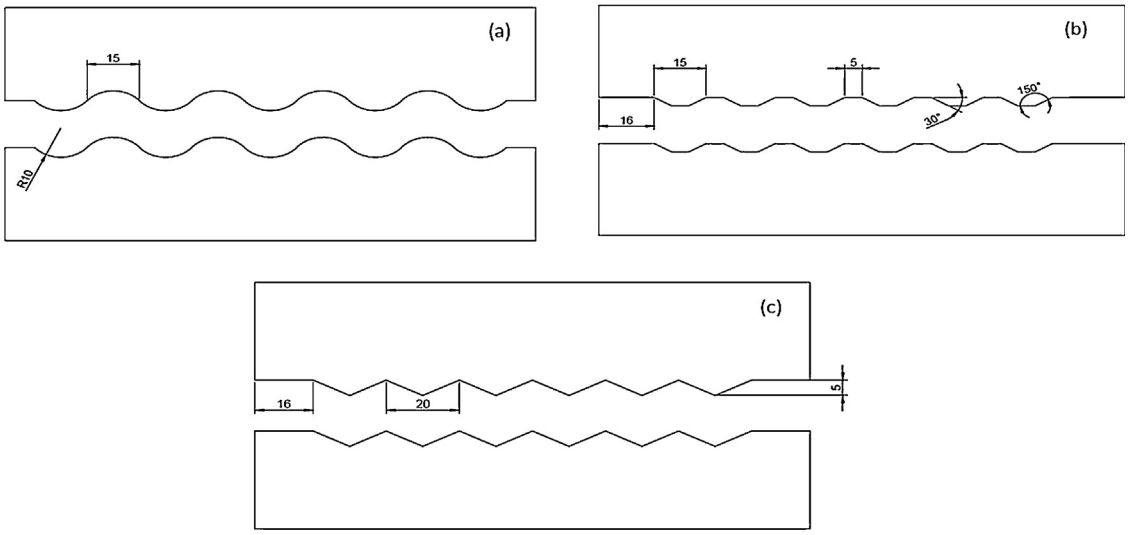

Fig. 1 – Different die profiles used for the corrugation.

strains experienced at given locations. The difference in the strain values according to the two routes of estimation indicates the degree of localization of the severe plastic deformation experienced by the samples as a function of the die profile.

3. Characterization

Microhardness testing using a Wilson Wolpert (Germany) hardness tester with a diamond indenter, a load of 9.8 N and an indenting speed of 5 mm/s was done on the processed samples at ten different locations at regular intervals along the length of the samples with a view to ascertaining the hardness variation along the sheet length direction. Tensile tests on the processed materials as per ASTM standard E8M, with a ram velocity of 2.5 mm/s were conducted using a servo-hydraulic INSTRON universal testing machine.

Electron backscatter diffraction (EBSD) analysis was used to study the microstructure, grain size distribution and grain boundary misorientation angles in the parent as well as the processed samples. The samples were prepared by polishing them well by SiC emery sheets of 300, 600, 1000, 1200 mesh grids followed by suspended alumina polishing and colloidal silica polishing. In case of every corrugation die, characterization was done after every two passes.

Fig. 2 – Schematic view of hydraulic press with heating chamber mounted and thermocouple with a PID controller.

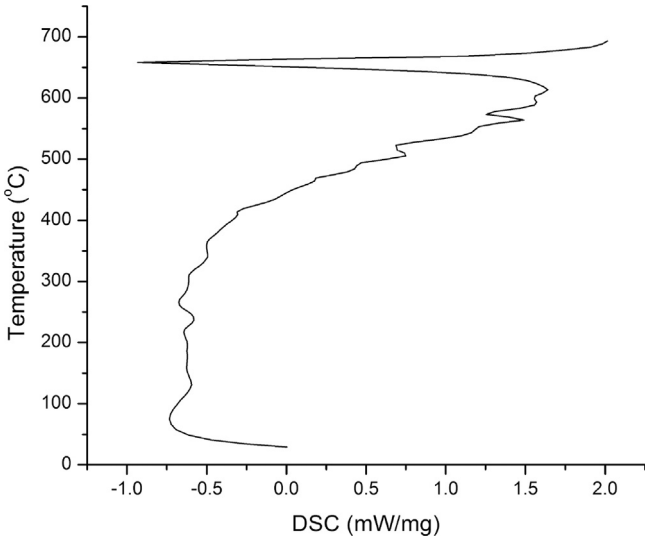

Fig. 3 – DSC curve for the AA8090 AL-Li alloy.

Manual polishing down to 100 μm thickness was followed by thinning to 100 nm using ion milling and dimple finishing. Transmission Electron Microscopy (TEM) was used to understand the mechanism of grain refinement during the RCS process by examining dislocations generated, disappearance of original grain boundaries, dynamic recovery and dynamic recrystallization.

4. Results and discussion

4.1. *Microhardness*

The average hardness value of the as-received material (AA8090) is 75 ± 1 HV. The hardness uniformity or its absence in the samples processed using each of the dies for different number of passes was compared after the 2nd, 6th, 10th and higher passes. The closeness and uniformity of hardness reveals uniform grain size in the specimens. Fig. 4(a) displays the hardness variation for the samples processed through the semi-circular die, flat groove die and V-groove die after the second pass. Only a marginal improvement in the hardness values is noticed, i.e., the samples processed through the semi-circular die had a hardness of 77 ± 1 HV, flat groove die 77 ± 2 HV and V-groove die 81 ± 1.5 HV. The scatter in the values of the hardness is lower in the samples processed by the semi-circular die due to its smooth profile and the absence of sharp changes in cross-section. The latter feature lowers the values of the stress concentration. Fig. 4(b) presents the hardness plots of the samples processed through every die after six passes. The average hardness values of the samples processed through the semi-circular and the flat groove dies were 80 ± 2 HV and the samples processed through the V-groove die had a higher average hardness of 88.5 ± 1 HV. The hardness variations in all the samples were rather small. Fig. 4(c) shows the hardness plots for samples subjected to 10 passes. The average hardness values of the samples processed through a semi-circular die is 82.5 ± 1.5 HV, for a flat groove die it is 85 ± 2.5 HV and for a V-groove die it is 98 ± 2.5 HV. Variation in the hardness value increases with the number of the pass, but still it is rather small. Fig. 4(d) shows the hardness plot of samples which could survive without breaking beyond the 10th pass. However, a large scatter in the hardness plot is observed due to surface cracking in samples subjected to these many number of passes. Relatively substantial increase in hardness is present in case of the semi-circular die after 16 passes, i.e., 88 ± 2 HV and after 12 passes in case of the flat groove die, the hardness was 91.5 ± 3.5 HV. In case of the V-groove die, after the 10th pass the sample displayed an average hardness of 98 ± 2.5 HV, which was higher than the hardness values recorded in the specimens processed through the other dies even after more number of passes. This is due to the formation of a much larger number of shear bands in case of the V-groove die (more severe strains) [20]. An examination of Table 1 reveals that the strain imparted per pass is the maximum for the V-groove die, medium for the semi-circular die and the least for the flat groove die. As a result, failure due to surface crack formation was seen earlier (14th pass) in case of the flat groove die compared with the semi-circular die (16th pass). This leads to a conclusion that a semi-circular die design is preferable to a flat groove die for imparting more uniform strains. The V-groove die leads to more strain before the appearance surface cracks than the flat groove die, notwithstanding the fact that with the former surface cracks appeared earlier after the 12th pass itself. Among the three designs studied, the semi-circular die gave rise to the largest cumulative strain, yet the hardness value produced in the V-groove die was the maximum, which was followed by that of the flat groove die, with the hardness of the material which was

Table 1 – Imparted strain in each of the die after different number of passes.

No. of passes	Semi circular die		Flat grooved die		V-grooved die	
	By experiment	By formula	By experiment	By formula	By experiment	By formula
2	0.096	.712	0.092	0.692	0.133	1.856
4	0.163	1.424	0.137	1.384	0.233	3.712
6	0.225	2.136	0.2	2.076	0.283	5.568
8	0.293	2.848	0.267	2.760	0.35	7.424
10	0.388	3.56	0.325	3.46	0.383	9.280
12	0.514	4.272	0.35	4.152	Fractured	
14	0.527	4.984	Fractured			
16	0.533	5.697				
17	Fractured					

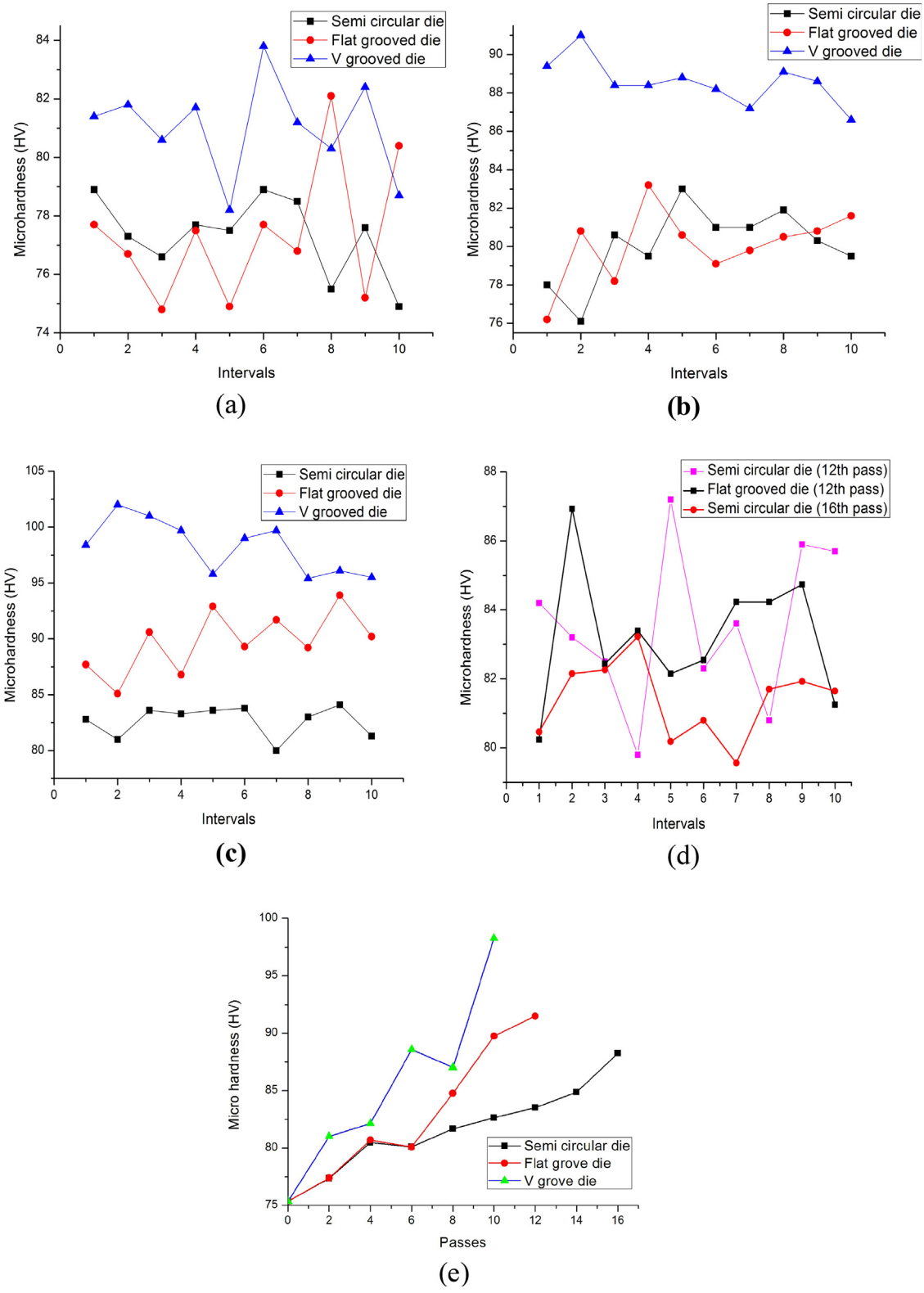

Fig. 4 – Hardness distribution in the samples (a) after 2 passes, (b) after 6 passes, (c) after 10 passes, (d) after a higher number of passes (>10 passes), (e) hardness comparison chart.

subjected to RCS through a semi-circular die being the lowest. This point needs further probing because the results seem to suggest that in addition to the amount of strain suffered, the distribution of strain (which could affect recovery processes differently depending on its nature) is also important in determining the resulting hardness.

Even after several passes, in case of all the three die profiles the hardness distribution was homogeneous, with only a small

scatter. As a result, the grain size distribution was also nearly uniform. Marginal improvement in hardness was noted after intermediate number of passes. Fig. 4(e) compares the hardness value as a function of the die profile. From the results it is found that the AA 8090 alloy in RCS processing for the chosen profile dimensions could enhance its hardness by 17% using the semicircular die, 21% using the flat groove die and 30% using the V-groove die.

4.2. *Tensile strength*

The as-received material in the annealed condition (a surmise based on the hardness value and the microstructure) has an ultimate tensile strength (UTS) of 190 MPa and a failure strain of 12.5%. Fig. 5(a) shows the stress–strain plot for specimens processed by different number of passes using the semi-circular die. For comparison, the stress–strain plot of parent material also is included. It is clear that the tensile strength increases up to the end of the 12th pass, while at the same time there was a decrease in the elongation at fracture. Beyond this point surface cracks appeared on the samples, which led to a loss in both strength and elongation. A maximum strength of 279 MPa was obtained after the 10th pass. The hardness with respect to the number of passes has an increasing trend throughout. However, the trend for the tensile strength was different. The hardness, being a highly localized measurement, is not affected significantly by surface cracks, which appear at significant intervals, but it has a noticeable effect on the tensile strength. The flat groove profile could provide a shear stress in addition to a normal stress. Therefore, the specimen experiences a more severe plastic strain compared with the semi-circular die (see Table 1). Hence, dislocation generation during the initial passes is more for the former. In case of the flat groove die, the UTS increases with the number of passes up to 8 passes and decreases after the 10th and the 12th pass (Fig. 5(b)). The UTS values for the first two passes are higher due to strain hardening, which increases sharply in the early passes. After the later passes, the increase in the UTS is due to the formation of near-stable grains (briefly explained in Section 4.3), which tends to flatten the stress–strain curve. In the case of corrugations using a V-groove die, the specimen underwent the minimum number of passes before the development of surface cracks and the nudging effect due to the sharp V edges had assumed importance. This die profile could impart a higher strain compared with the semi-circular die and the flat groove die due to its maximum volume shear (see Table 1). Fig. 5(c) shows the stress–strain plots for the specimen processed using a V-groove die. Consistent with the

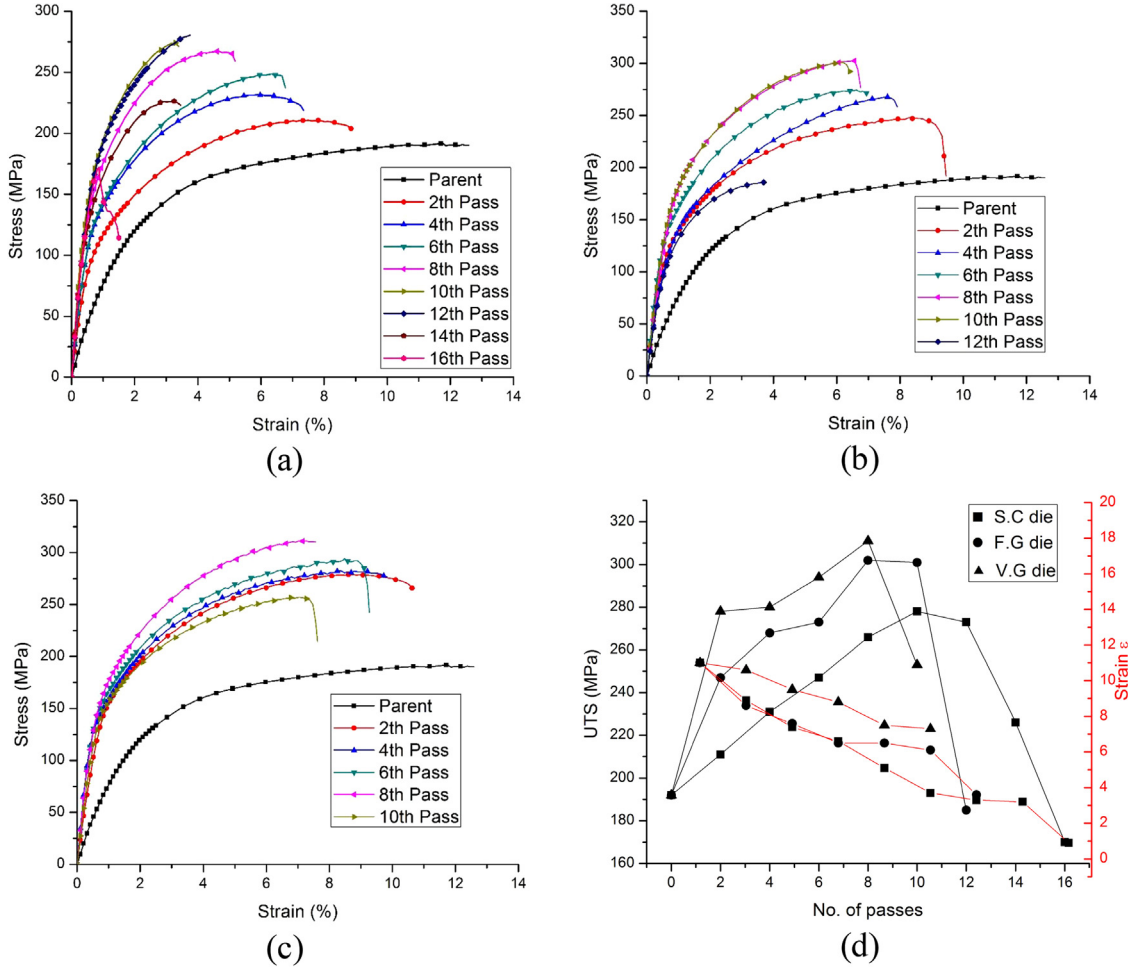

Fig. 5 – Stress–strain curves for samples processed to different extent (a) using a semicircular die, (b) using a flat groove die, (c) using a V-groove die. (d) Ultimate stress and failure strain comparison chart.

above argument, the stress–strain curve after the 8th pass exhibits a high UTS value (311 MPa).

A general problem in RCS is that at pre-failure passes (i.e., the samples processed close to the maximum number of passes before the specimen fractures into two or more pieces during RCS), the ultimate strength drops compared with the preceding passes due to the development of surface cracks. The tensile stress–strain plots of specimens processed by the different dies reveal that the samples processed using the V-groove die have a better combination of properties compared with the samples processed using the other dies, i.e., the UTS improvement compared to the parent material is 63.5%, while also retaining 60% of the original plasticity after the 8th pass. In contrast, the samples processed using a semi-circular die has shown a maximum UTS improvement of 46.8%, and it retains only 26.4% of its original plasticity after the 12th pass. The samples processed using a flat groove die produced a maximum UTS increase of 59% and it retains 52.8% of its original plasticity after the 10th pass. Figures also show that the yield strength has improved in the samples processed using a semi-circular die and a flat groove die, but has remained the same in the samples processed using a V groove die. (The parent material has a yield strength of 90 MPa.) This means that work hardening and stability of flow is more robust when a V groove die is used. The UTS and stain comparison chart for all the three dies have been given in Fig. 5(d).

4.3. *EBSD analysis*

The EBSD orientation map and the texture present in the parent material are shown in Fig. 6(a). The same features corresponding to the processed samples under conditions where sound properties are obtained, i.e., after 12 passes using a semicircular die (Fig. 6(b)), after 10 passes using a flat groove die (Fig. 6(c)) and after 8 passes using a V-groove die (Fig. 6(d)) are also shown. The colors of EBSD map indicate the orientation of the grains represented in the picture. The grain size was calculated by the integrated system attached to the EBSD setup by taking the scanned area and density of high-angle grain boundaries into account. The parent material has an average grain size of 65 μm. On the other hand, the processed materials have the following average grain size values: 38 μm after 12 passes using a semicircular die; 44 μm after 10 passes using a flat groove die; and 12 μm after 8 passes using a V-groove die.

Grain boundary character distributions in the different samples are given in Fig. 7. Fig. 7(a) presents the misorientation angle distribution for the parent material. Fig. 7(b)–(d) displays the misorientation angle fractions of samples processed using the semicircular die for 12 passes, using a flat groove die for 10 passes and a V-groove die for 8 passes respectively. The specimens processed using the V-groove die have a greater fraction of high-angle grain boundaries

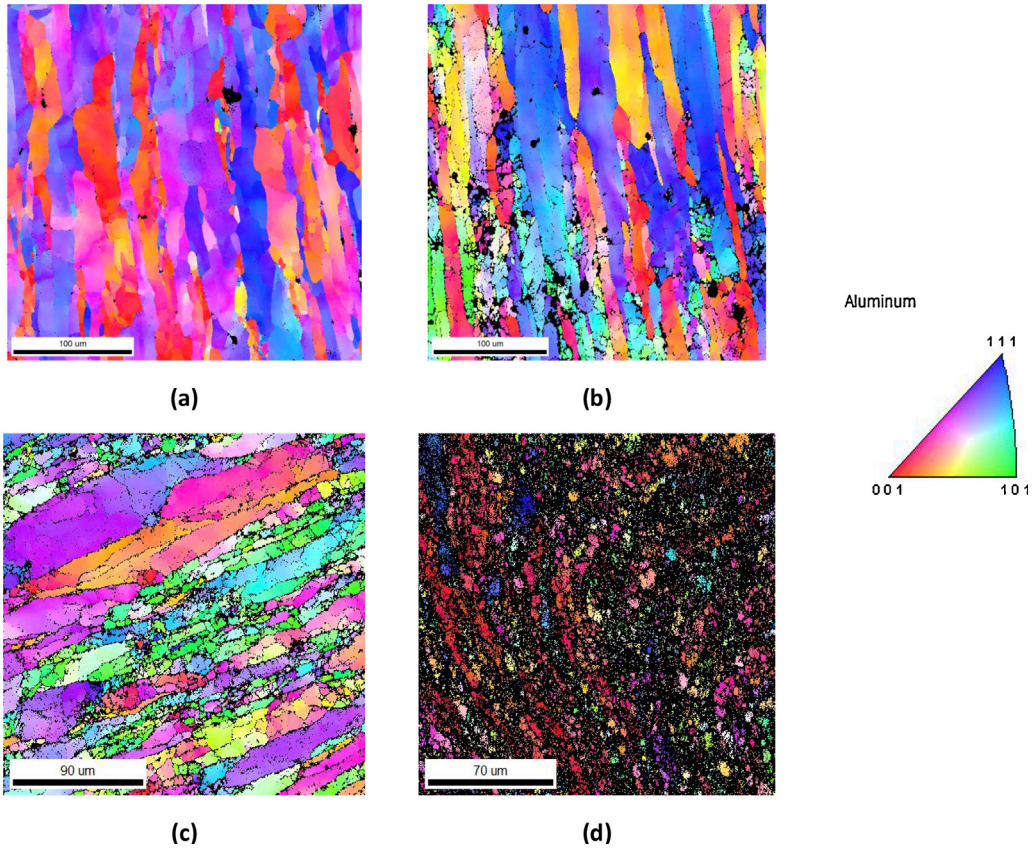

Fig. 6 – EBSD orientation maps of (a) parent material, (b) after 12 passes using a semi-circular die, (c) after 10 passes using a flat groove die, (d) after 8 passes using a V-groove die.

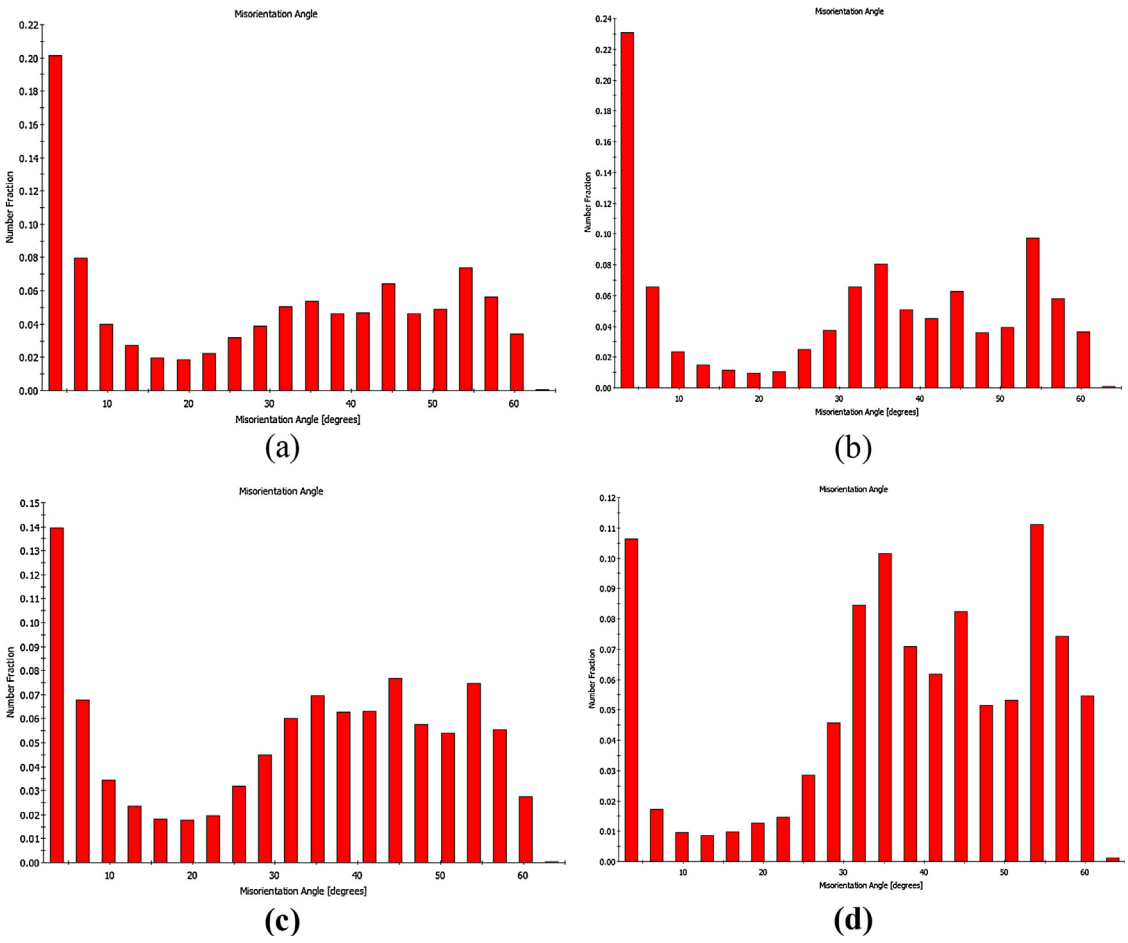

Fig. 7 – Misorientation angle of (a) parent material, (b) after 12 passes through a semi-circular die, (c) after 10 passes through a Flat groove circular die, (d) after 8 passes through a V-groove die.

compared with the fractions for the other die profiles. It is known that the determination of the grain boundary character distribution, development of preferred orientation etc. becomes questionable when the grain size becomes ultrafine tending to a nanostructure. At grain sizes encountered in this study there is not likely to be much uncertainties associated with the present measurements [23].

The grain size distributions are given in Fig. 8. The grain size distribution reveals information about localized grain refinement over short ranges. Fig. 8(a) shows the grain size distribution present in the parent material. The grain size distribution of samples processed through a semi-circular die for 12 passes is presented in Fig. 8(b) which indicates that an increasing area fraction of refined grains has come into being. There is also evidence for small string formation. Fig. 8(c) displays the grain size distribution in a sample subjected to 10 passes using a flat groove die. The size distribution ranges from the micron to the ultrafine grain size range. Fig. 8(d) shows the grain size distribution in a sample that has undergone 8 passes through a V-groove die. Evidently, the curve has shifted toward the ultrafine grain size range, i.e., more fine grains of size less than 1 μm are present compared with those pertaining to the other die profiles. This observation explains clearly why a sample processed using a V groove die has a higher strength and hardness than those found for other die profiles (Hall–Petch effect).

The processing of samples in RCS is often divided into three segments. The strengthening effect in the first segment is due to strain hardening and bulging of stable grain boundaries [24], the strengthening effect in the second segment is due to sub-grain formation due to a combination of dislocation annihilation [25] and dislocation reorientation [26], and in third segment, the strengthening is due to stable grain/grain boundary formation due to a considerable increase in the density of dislocations at the boundaries. From Table 1 it is clear also that the strain imparted on the specimen by the V-groove die in each pass is greater than that imparted by the other die profiles. In contrast, dislocation generation during the initial passes is high which leads to sub-grain formation. At higher number of passes, more and more dislocations enter the grain boundaries and cause the formation of stable grains having high-angle boundaries. It is understandable that in view of the largest strain imparted in case of the V-groove die, the high-angle grain boundary fraction is also the largest in this case.

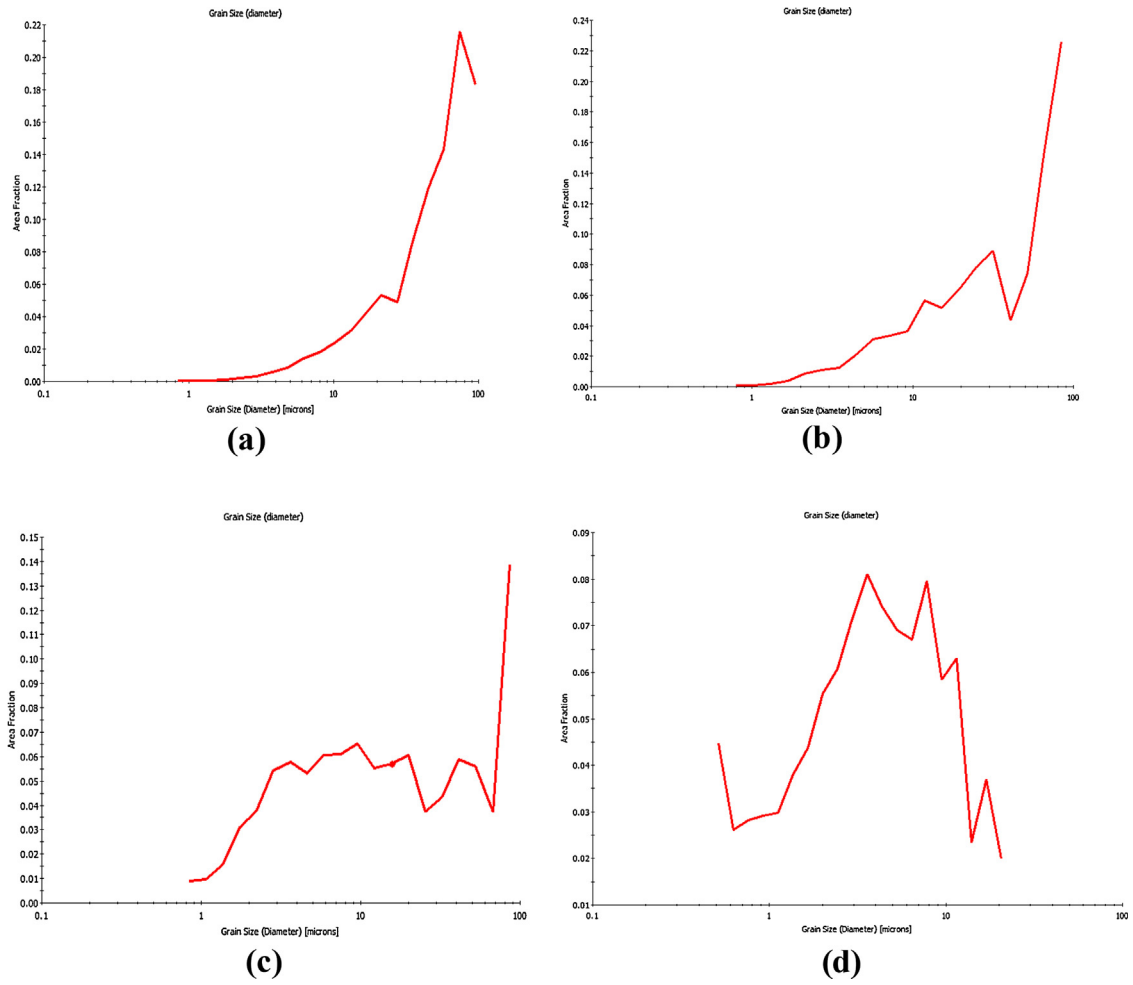

Fig. 8 – Grain size distribution of (a) parent material, (b) after 12 passes through a semi-circular die, (c) after 10 passes through a flat groove die, (d) after 8 passes through a V-groove die.

4.4. *TEM analysis*

TEM images were taken in a plane of the sample perpendicular the pressing direction for the parent material as well as the sample processed using a V groove die – Fig. 9. The Al_3Li precipitated phase is marked by a white box in the figures. The parent material has coarse grains, with extremely small amounts of Al_3Li (Fig. 9(a)). Fig. 9(b) confirms that the initial passes give rise to extensive dislocation generation inside the grains and dislocation pile-ups, as reported earlier [27]. Both lead to strain hardening. Fig. 9(c) shows the accumulation of dislocations after the intermediate passes, i.e. after 4 passes. Fig. 9(d) taken after 6 passes seems to suggest that the dislocations are pinned by the Al_3Li precipitates. The Al_3Li precipitates are highlighted in the TEM images. Fig. 9(e) shows the refined grain structure of AA8090 alloy after 8 passes. The least identified thick extinction contours (indicative of the presence of a strain field) in the grain boundaries show the movement of dislocation toward the grain boundaries [28], which indicates the initiation of dynamic recrystallization (DRC). The conversion of the sub-grains to high-angle grain boundaries on the lines described earlier is likely to be responsible for this observation. In Fig. 9(f), taken after 10 passes, evidence for the commencement of continuous dynamic recrystallization (CDRC) is seen, where no grain boundaries or dislocations could be witnessed. However, the grain boundaries dissolve during CDRC, but the oriented precipitates have not been redistributed into the matrix. Instead, an array or network of precipitated Al_3Li-like agglomeration is spotted in Fig. 9(f). The bulging of high-angle grain boundaries assists the elongated grains to acquire a near-equiaxed shape after severe plastic deformation. It is also evident from the present study that the V-groove die gives the best grain refinement. In the absence of surface cracking, more number of passes would have been possible and the grain refinement would have been more. By fileting the die corners and the rounding off of the V-configuration, it should be possible to decrease stress concentration during deformation. In such a situation further grain refinement would be possible. This, in our opinion, is a worthwhile pursuit because the grain refinement that can be achieved using the other SPD processes, e.g., ECAP, HPT, is considerably greater.

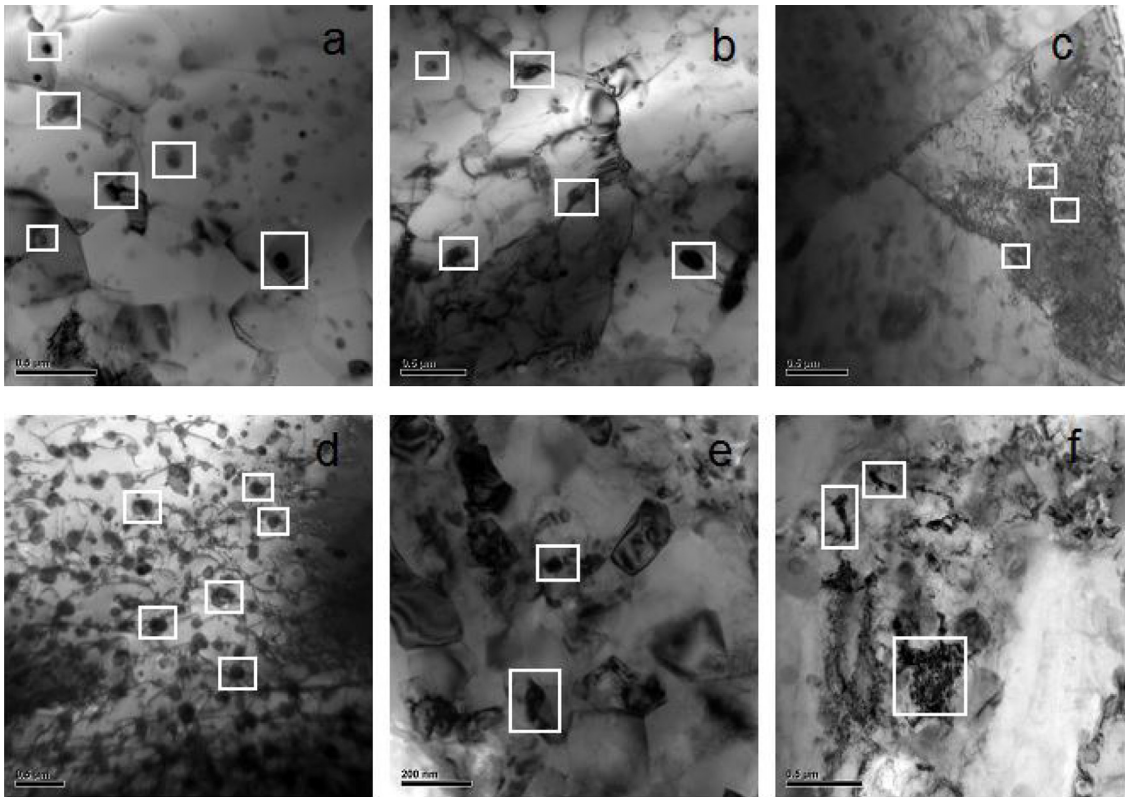

Fig. 9 – HRTEM images of (a) the parent material, (b) after 2 passes through a V-grooved die, (c) after 4 passes through a V-grooved die, (d) after 6 passes through a V-grooved die, (e) after 8 passes through a V-grooved die, (f) after 10 passes through a V-grooved die.

5. Conclusions

As Al-Li alloy AA8090 could not be deformed at 200 °C or lower temperatures, the present study was carried out at 300 °C, below the recrystallization temperature of the alloy. This experimental study led to the following observations.

AA8090 Al-Li alloy sheets could be successfully processed using different die profiles and the resultant grain refinement was highly dependent on the die profile.

Among the dies used, the V-groove die induces a high volume shear which leads to severe plasticity. As a result, ultrafine grains are formed. The difference between the actual strain and the calculated strain clearly establishes the non-uniform and localized nature of severe plastic deformation. The measured strain in a sample processed using a V-groove die, in which grain refinement was maximal, shows a substantial deviation from the theoretically calculated strain.

Micro-hardness distribution in the samples processed using a V-groove die is 30% higher than that of the parent material and nearly uniform throughout the sample and the hardness values are more than in the samples processed using the other two dies.

Good property improvement was achieved after 8 passes through a V-groove die and the grain size had reduced to 12 μm from an initial value of 65 μm and the UTS had improved by 63%.

The EBSD results show that the samples processed using a V-groove die for 8 passes contain ultrafine grains possessing high-angle grain boundaries. The increased strength observed is a manifestation of the Hall–Petch effect.

From the TEM analysis it is understood that the dislocations get initiated at the grain boundaries and the interfaces of Al_3Li precipitates during the initial passes. Multiplication of dislocations, reorientation of precipitates and formation of sub-grains in the intermediate passes and grain refinement with formation of high-angle grain boundaries after a higher number of passes were the other features detected.

Acknowledgements

J. Jenix Rino wishes to thank University Grant Commission, Government of India for the grant of a research fellowship (MANF-2013-14-CHR-TAM-30573). S. Balasivanandha Prabu gratefully acknowledges Grant No. SB/FTP/ETA-104/2012, received from the Science & Engineering Research Board, Department of Science and Technology, Government of India. The authors thank Prof. Indradev Samajdar, IIT Bombay, for extending the EBSD facility and also PSG College of Technology, Coimbatore, India for allowing the use of the HRTEM facility. Finally, the authors thank ALCOA (Germany) for the supply of the AA8090 Al-Li alloy used in this study.

REFERENCES

[1] S. Bagherifard, R. Ghelichi, A. Khademhosseini, M. Guagliano, Cell response to nanocrystallized metallic substrates obtained through severe plastic deformation, ACS Applied Materials & Interfaces 6 (2014) 7963–7985.

[2] A. Azushima, R. Kopp, A. Korhonen, D.Y. Yang, F. Micari, G.D. Lahoti, et al., Severe plastic deformation (SPD) processes for metals, CIRP Annals – Manufacturing Technology 57 (2008) 716–735.

[3] Y.T. Zhu, T.C. Lowe, Observations and issues on mechanisms of grain refinement during ECAP process, Materials Science and Engineering: A 291 (2000) 46–53.

[4] A.P. Zhilyaev, S. Lee, G.V. Nurislamova, R.Z. Valiev, T.G. Langdon, Microhardness and microstructural evolution in pure nickel during high-pressure torsion, Scripta Materialia 44 (2001) 2753–2758.

[5] Y. Saito, H. Utsunomiya, N. Tsuji, T. Sakai, Novel ultra-high straining process for bulk materials—development of the accumulative roll-bonding (ARB) Process, Acta Materialia 47 (1999).

[6] M. Noda, M. Hirohashi, K. Funami, Low temperature superplasticity and its deformation mechanism in grain refinement of Al-Mg alloy by multi-axial alternative forging, Materials Transactions 44 (2003) 2288–2297.

[7] Y. Beygelzimer, D.V. Orlov, V.N. Varyukhin, A new severe plastic deformation method: twist extrusion, in: Y.T. Zhu, T. G. Langdon, R.S. Mishra, S.L. Semiatin, M.J. Saran, T.C. Lowe (Eds.), Ultrafine Grained Materials II. Proceedings of a Symposium, Held During the 2002 TMS Annual Meeting I, Seattle, Washington, February 17–21, (2002) 297–304.

[8] Y. Xu, L. Hu, Y. Sun, J. Jia, J. Jiang, Q. Ma, Microstructure and mechanical properties of AZ61 magnesium alloy prepared by repetitive upsetting-extrusion, Transactions of Nonferrous Metals Society of China 25 (2015) 381–388.

[9] J.C. Kim, Y. Nishida, H. Arima, T. Ando, Microstructure of Al-Si-Mg alloy processed by rotary-die equal channel angular pressing, Materials Letters 57 (2003) 1689–1695.

[10] M. Richert, Q. Liu, N. Hansen, Microstructural evolution over a large strain range in aluminium deformed by cyclic-extrusion – compression, Materials Science and Engineering: A 260 (1999) 275–283.

[11] W. Guo, Q. Wang, B. Ye, H. Zhou, Microstructure and mechanical properties of AZ31 magnesium alloy processed by cyclic closed-die forging, Journal of Alloys and Compounds 558 (2013) 164–171.

[12] Y.T. Zhu, L. Alamos, T.C. Lowe, S. Fe, H. Jiang, J. Huang, United States Patent US006197129B1, 2001.

[13] Y. Estrin, A. Vinogradov, Extreme grain refinement by severe plastic deformation: a wealth of challenging science, Acta Materialia 61 (2013) 782–817.

[14] N. Thangapandian, S.B. Prabu, The role of corrugation die parameters on the mechanical properties of aluminum alloy (AA 5083) processed by repetitive corrugation and straightening, Journal of Materials Science and Chemical Engineering (2015) 208–212.

[15] H.Y. Li, W. Kang, X.C. Lu, Effect of age-forming on microstructure, mechanical and corrosion properties of a novel Al–Li alloy, Journal of Alloys and Compounds 640 (2015) 210–218.

[16] T.H. Sanders, Coarsening of δ′(Al_3Li) Precipitates in Aluminum-Lithium Alloys. AD-A243 478, Naval Air Development Center Report, 1983.

[17] H. Ovri, E.T. Lilleodden, New insights into plastic instability in precipitation strengthened Al-Li alloys, Acta Materialia 89 (2015) 88–97.

[18] N. Llorca-Isern, P.A. Gonzalez, C.J. Luis, I. Laborde, Severe plastic deformation of a commercial aluminium-lithium alloy (AA8090) by equal channel angular pressing, Materials Science Forum 503–504 (2006) 871–876.

[19] C. Gao, Y. Luan, J.C. Yu, Y. Ma, Effect of thermo-mechanical treatment process on microstructure and mechanical properties of 2A97 Al-Li alloy, Transactions of Nonferrous Metals Society of China (English Edition) 24 (2014) 2196–2202.

[20] N. Thangapandian, S. Balasivanandha Prabu, K.A. Padmanabhan, Effects of die profile on grain refinement in Al–Mg alloy processed by repetitive corrugation and straightening, Materials Science and Engineering: A 649 (2016) 229–238.

[21] H. Sheikh, E. Paimozd, S.M. Hashemi, Work hardening of Duratherm 600 cobalt superalloy using repetitive corrugation and straightening process, Russian Journal of Non-Ferrous Metals 51 (2010) 59–61.

[22] G.G. Niranjan, U. Chakkingal, Deep drawability of commercial purity aluminum sheets processed by groove pressing, Journal of Materials Processing Technology 210 (2010) 1511–1516.

[23] A. Kauffmann, J. Freudenberger, H. Klauß, V. Klemm, W. Schillinger, V. Subramanya Sarma, et al., Properties of cryo-drawn copper with severely twinned microstructure, Materials Science and Engineering: A 588 (2013) 132–141.

[24] B. Shen, L. Deng, X. Wang, A new dynamic recrystallisation model of an extruded Al-Cu-Li alloy during high-temperature deformation, Materials Science and Engineering: A 625 (2015) 288–295.

[25] C. Wang, F. Li, B. Chen, Z. Yuan, H. Lu, Severe plastic deformation techniques for bulk ultrafine-grained materials, Rare Metal Materials and Engineering 41 (2012) 941–946.

[26] A. Mishra, B. Kad, F. Gregori, M. Meyers, Microstructural evolution in copper subjected to severe plastic deformation: experiments and analysis, Acta Materialia 55 (2007) 13–28.

[27] E. Hosseini, M. Kazeminezhad, Stress-based model on work hardening and softening of materials at large strains: corrugation process of sheet, Journal of Materials Science 44 (2009) 1212–1218.

[28] N. Thangapandian, S. Balasivanandha Prabu, K.A. Padmanabhan, Effect of temperature and velocity of pressing on grain refinement in AA5083 aluminum alloy during repetitive corrugation and straightening process, Metallurgical and Materials Transactions A 47 (2016) 6374–6383.